Journal of Materials Chemistry A

PAPER

View Article Online
View Journal | View Issue

Cite this: J. Mater. Chem. A, 2015, 3, 10551

Thermostable and nonflammable silica–polyetherimide–polyurethane nanofibrous separators for high power lithium ion batteries†

Yunyun Zhai,[ab] Ke Xiao,[a] Jianyong Yu,[c] Jianmao Yang[d] and Bin Ding*[ac]

Received 2nd February 2015
Accepted 10th April 2015

DOI: 10.1039/c5ta00856e

www.rsc.org/MaterialsA

Safety remains a practical concern in lithium ion batteries (LIBs), which is closely associated with the internal shorting caused by the poor dimensional thermostability at elevated temperature and the flammability of separators. Here, we report a novel strategy to fabricate thermostable and nonflammable silica–polyetherimide–polyurethane (SiO_2–PEI–PU) nanofibrous membranes *via* an electrospinning process. Benefiting from the high porosity, interpenetrating network structure and synergetic effect of silica nanoparticles, PEI and PU, the as-prepared SiO_2–PEI–PU membranes exhibit uniform pore size distribution, high ionic conductivity (6.25 mS cm^{-1}) and good electrochemical stability up to 4.86 V. Notably, the hot oven and combustion tests reveal that the SiO_2–PEI–PU membranes possess improved thermostability displaying 2% dimensional change after exposure to 170 °C for 0.5 h and flame retardant properties, which could be beneficial for improving the safety of LIBs. Significantly, the SiO_2–PEI–PU membrane based Li/$LiFePO_4$ cell exhibits more excellent cyclability delivering a discharge capacity of 158.91 mA h g^{-1} at the 90th cycle and better rate capability compared with the cell based on the Celgard membrane. Meanwhile, the SiO_2–PEI–PU membrane based Li/$LiFePO_4$ cell also shows more excellent cell performance even at an elevated temperature of 60 °C. The results clearly demonstrate that the SiO_2–PEI–PU membranes are promising separator candidates, which will also pave the way for further application of nanofibrous membranes in high power LIBs.

Introduction

Safety becomes a primary concern for commercial development of high-rate and high capacity lithium ion batteries (LIBs) in hybrid electric vehicles and electric vehicles. Most of the unsafe events are closely related to the poor thermal stability of separators, which could trigger internal shorting at elevated temperature. Among the major battery components, separators not only play an important role in preventing the physical contact between the cathode and anode electrodes to avoid short circuit but also serve as the electrolyte reservoir to enable free ionic transport *via* liquid electrolyte-filled pores.[1–3] Nowadays, commercial separators are usually made up of porous polyolefin membranes owing to their high mechanical strength, good electrochemical stability and thermal shutdown performance.[2] Nevertheless, the intrinsic features of polyolefin, such as poor thermal stability at a high temperature (150 °C) due to the relatively low softening and melting temperatures, and sluggish ionic transport caused by low porosity and poor electrolyte affinity, restrict their applications in high power LIBs.[4] Therefore, it is highly desirable to fabricate membranes with enhanced thermostability and high ionic conductivity to guarantee the safety and reliability of LIBs.

In an effort to solve the above-mentioned problems, electrospun nanofibrous membranes, such as polyimide,[5,6] polyvinylidene fluoride and its copolymer,[7–9] polymethylpentene,[10] polyacrylonitrile,[11,12] and nylon 6,6,[13] have been extensively investigated due to their high ionic conductivity brought about by high porosity and interconnected pore structure.[14–16] Although some of these separators exhibit good dimensional thermostability, their combustion behaviors have not been studied previously. Meanwhile, there still exists some possibility of causing internal shorting and thus deteriorating the battery performance due to the intrinsic large pore size of electrospun membranes. Thus, the fabrication of thermostable nanofibrous membranes with a controllable pore size is still a challenging problem.

[a]State Key Laboratory for Modification of Chemical Fibers and Polymer Materials, College of Materials Science and Engineering, Donghua University, Shanghai 201620, China. E-mail: binding@dhu.edu.cn

[b]College of Biological, Chemical Sciences and Engineering, Jiaxing University, Jiaxing 314001, China

[c]Key Laboratory of Textile Science & Technology, Ministry of Education, College of Textiles, Donghua University, Shanghai 201620, China

[d]Research Center for Analysis and Measurement, Donghua University, Shanghai 201620, China

† Electronic supplementary information (ESI) available: Stress–strain curves of the Celgard membrane, and FT-IR spectra and EDX spectra of SiO_2–PEI–PU nanofibrous membranes. See DOI: 10.1039/c5ta00856e

Inorganic nanoparticles like silica (SiO_2) and zirconium dioxide have been used to fabricate separators for LIBs because they can promote ionic conductivity, thermal stability and compatibility with lithium metal.[17–19] Polyetherimide (PEI) is an amorphous polymer with carboxyl (C═O) and oxy-ether (–O–) groups in its molecular structure, which possesses high chemical stability, good dimensional stability and inherent flame resistance;[20,21] thus it is a promising candidate for fabricating thermostable and nonflammable separators. Polyurethane (PU), a class of thermoplastic polymer that contains soft segments and hard segments, is used to prepare separators with high ionic conductivity because the soft segments do not form ionic clusters after being dissolved in an alkali metal.[22] We have recently reported that hierarchical structured silica nanoparticle coated polyetherimide–polyurethane nanofibrous composite membranes are obtained by electrospinning followed by a dip-coating process.[23]

In this work, we present our continuous efforts to fabricate thermostable and nonflammable SiO_2–PEI–PU nanofibrous separators with a controllable pore structure *via* a one-step electrospinning technique. The key to our development design is that the use of PEI endows the as-prepared membranes with not only improved thermostability and flame retardancy but also excellent affinity to liquid electrolytes. The SiO_2–PEI–PU membranes demonstrate high ionic conductivity, improved thermal stability and uniform pore size distribution due to the introduction of SiO_2 nanoparticles. Our work presents the feasibility of electrospun nanofibrous membranes to solve the safety problems of high power LIBs.

Experimental

Materials

Polyetherimide (PEI, Ultem 1000, Saudi Basic Industries Corporation) was purchased from Dongguan Jiangxin Plastic Co., Ltd., China. Polyurethane (PU, Elastollan 2280A10) was supplied by BASF Co., Ltd. Silica nanoparticles (SiO_2 NPs, diameter of particles, 7–40 nm, specific surface area, 120 $m^2\ g^{-1}$) were obtained from Aladdin Chemistry Co. Ltd. *N*,*N*-Dimethylformamide (DMF) was bought from Shanghai Lindi Chemical Reagents Co., Ltd., China. The Celgard 2320 membrane (Celgard, China) with a thickness of about 20 μm was used as a comparison sample. All chemicals were of analytical grade and used as received without further purification.

Fabrication of SiO_2–PEI–PU nanofibrous membranes

To prepare 7 wt% SiO_2–PEI–PU blended solutions, different amounts of SiO_2 NPs (0, 2, 5, 8, and 11 wt% based on the weight of PEI–PU) were ultrasonically dispersed into DMF for 10 min, respectively, followed by the addition of a certain amount of PEI–PU (1/1, w/w) under vigorous stirring for another 12 h. The above-mentioned SiO_2–PEI–PU blended solutions were loaded into a 10 mL syringe and injected through a plastic needle at a feed rate of 1 mL h^{-1} by using a DXES-3 spinning equipment (Shanghai Oriental Flying Nanotechnology Co., Ltd., China). A high voltage of 30 kV was applied to the needle tip, and the distance from the spinneret to an aluminum foil-covered grounded rotating collector (rotating rate of 50 rpm) was 25 cm. The ambient temperature and relative humidity were 23 ± 2 °C and 45 ± 3%, respectively. Then, the resulting free-standing SiO_2–PEI–PU membranes with an average thickness around 50 μm were dried in a vacuum oven at 70 °C for 12 h to remove the residual solvent and transferred into a dry box for further use.

Characterization of SiO_2–PEI–PU nanofibrous membranes

The surface morphologies of the relevant membranes were studied by using a high resolution field-emission scanning electron microscopy (FE-SEM, S-4800, Hitachi Ltd., Japan). The average pore sizes and pore size distributions of the as-prepared membranes were measured by a bubble-point test using a capillary flow porosimeter (CFP-1100AI, Porous Materials Inc., USA). Porosities (P) of the resultant membranes were determined by using *n*-butanol uptake tests, which were calculated by the following equation:

$$P(\%) = \frac{M_{\mathrm{BuOH}}/\rho_{\mathrm{BuOH}}}{(M_{\mathrm{BuOH}}/\rho_{\mathrm{BuOH}}) + (M_{\mathrm{m}}/\rho_{\mathrm{m}})} \times 100 \quad (1)$$

where M_{BuOH} and M_{m} are the masses of *n*-butanol and dry membranes, respectively. ρ_{BuOH} is the density of *n*-butanol, and ρ_{m} is the density of dry membranes, which is calculated by the composition and true density of each component. The electrolyte uptakes were investigated by the weight difference of membranes before and after soaking in a liquid electrolyte (1 M lithium hexafluorophosphate ($LiPF_6$) dissolved in ethylene carbonate (EC)/ethyl methyl carbonate (EMC)/dimethyl carbonate (DMC) (1/1/1, w/w/w)) for 2 h, and then calculated according to the following equation:

$$\text{Uptake } (\%) = \frac{W_{\mathrm{w}} - W_{\mathrm{d}}}{W_{\mathrm{d}}} \times 100 \quad (2)$$

where W_{d} and W_{w} are the weights of the membranes before and after soaking in the electrolyte, respectively. The mechanical properties of the relevant membranes were evaluated on a tensile tester (XQ-1C, Shanghai New Fiber Instrument Co., Ltd., China), and the bendability was measured repeatedly under a longitudinal strain that ranged from 10 to 30 mm at a strain rate of 10 mm min^{-1}.[24] Fourier transform infrared (FT-IR) spectra were recorded with a Nicolet 8700 FT-IR spectrometer in the range of 4000–400 cm^{-1}. Energy-dispersive X-ray (EDX) measurements were conducted on a Philips Tecnai G2 F20 & a Hitachi S-4800. Thermal shrinkages were tested by storing the relevant membranes in an oven at various temperatures from 90 to 170 °C for 0.5 h, after that, dimensional changes of the membranes were carefully calculated by the following equation:

$$\text{Shrinkage } (\%) = \frac{A_0 - A}{A_0} \times 100 \quad (3)$$

where, A_0 and A are the areas of the relevant membranes before and after heat treatment, respectively.

Electrochemical performance evaluation

The ionic conductivity (σ) of relevant membranes was measured on liquid electrolyte-soaked membranes sandwiched between

two stainless steel (SS) blocking electrodes over the frequency range of 0.1 Hz to 1 MHz with an amplitude of 5 mV by the AC impedance method using a Zahner IM 6ex impedance analyzer. The ionic conductivity could be calculated from the following equation:

$$\sigma = \frac{d}{R_b \times S} \quad (4)$$

where d is the thickness of the relevant membranes, which was measured using an electronic micrometer (0.001 mm accuracy, CHY-C2 Thickness Tester, Labthink Co. Jinan, China), R_b is the bulk resistance obtained at the high frequency intercept of the Nyquist plot on the real axis, and S is the contact area between the membranes and the stainless steel blocking electrode. The MacMullin number (N_m) and tortuosity (τ) of membranes can be calculated by the following equations:

$$N_m = \frac{\sigma_0}{\sigma_{eff}} \quad (5)$$

$$\tau^2 = N_m P \quad (6)$$

where, σ_0 and σ_{eff} are the ionic conductivities of the liquid electrolyte (8.72 mS cm^{-1}) and liquid electrolyte soaked membranes, and P is the porosity of relevant membranes. The electrochemical stability windows of the liquid electrolyte-soaked membranes were determined by linear sweep voltammetry (LSV) using a working electrode of stainless steel and counter and reference electrodes of lithium metal at a scan rate of 2 mV s^{-1} over the potential range of 2.5 to 6.0 V *vs.* Li^+/Li.

Coin cells (2016-type) were assembled by sandwiching the separators between the $LiFePO_4$ cathode ($LiFePO_4$/carbon black/PVdF, 80/10/10, w/w/w) and the lithium metal anode. The mass loading of $LiFePO_4$ was about 8 mg cm^{-2}, much higher than that of most reported (about 2 mg cm^{-2}). The cyclability and C-rate capabilities of the Li/$LiFePO_4$ cells were investigated in a Land battery test system (CT 2001A, Wuhan Land Electronic Co. Ltd., China) in a potential range of 2.5 to 4.0 V at room temperature. All the assembly processes of cells were carried out in an argon-filled glovebox with oxygen and moisture level <1 ppm.

Results and discussion

Morphology and pore structure characteristics

Fig. 1a–e show the typical FE-SEM images of the as-prepared SiO_2–PEI–PU nanofibrous membranes with various SiO_2 contents (0, 2, 5, 8, and 11 wt%). The addition of SiO_2 particles does not change the fiber diameter significantly, and all the resultant membranes exhibit a tortuously interconnected porous structure constructed by randomly oriented fibers with an average diameter of 400–500 nm. But, the morphology becomes rougher when SiO_2 NPs are introduced (inset of Fig. 1b–e), these rough structures are generated by the wrinkles, nano-protrusions are formed by the SiO_2 NPs not only wrapped inside the fibers but also exposed on the fiber surface. Meanwhile, gradually increased wrinkles, nano protrusions and SiO_2 NPs are clearly visible on the fiber surface with increasing SiO_2 content, which are favorable to tune the pore structure of SiO_2–PEI–PU nanofibrous membranes. As can be seen in Fig. 1f, all the membranes have shown the pore size distributions in the range of 1.15–2.15 μm, and the average pore sizes decrease from 1.81 to 1.58 μm as the content of SiO_2 NPs increases (Table 1). It is worth noting that 77% pores of the as-prepared SiO_2–PEI–PU membranes containing 8 wt% SiO_2 NPs concentrate in the range of 1.5–1.7 μm, which confirms that SiO_2–PEI–PU membranes containing 8 wt% SiO_2 NPs possess uniform pore distribution to ensure a uniform current distribution throughout the membranes.

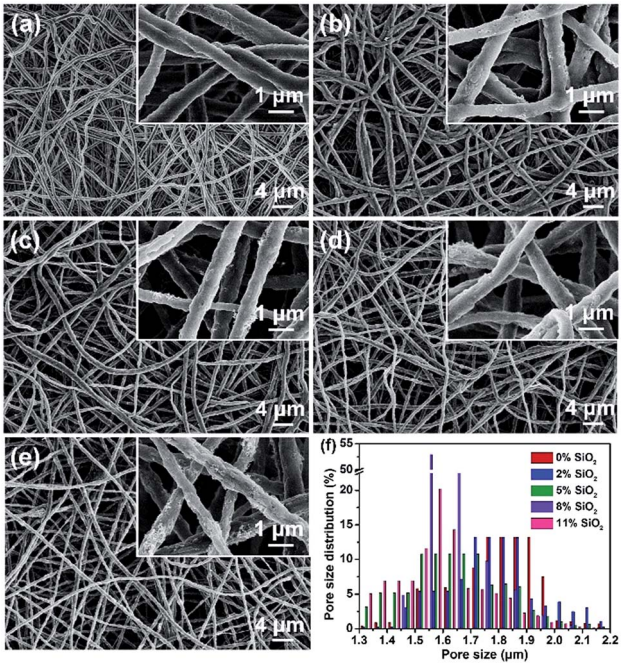

Fig. 1 FE-SEM images of the as-prepared SiO_2–PEI–PU membranes containing different SiO_2 contents (a) 0 wt%, (b) 2 wt%, (c) 5 wt%, (d) 8 wt%, and (e) 11 wt%. (f) Pore size distributions of the as-prepared SiO_2–PEI–PU membranes.

Porosity and electrolyte uptake

Table 1 also shows the porosities and electrolyte uptakes of the Celgard membrane and the as-prepared SiO_2–PEI–PU membranes with various SiO_2 contents. The porosities of the as-prepared membranes vary in the range of 80.66–84.97%, which are higher than the value of Celgard (49.83%) and SiO_2/nylon 6,6 membranes (70–77%).[13] The difference in porosity could be attributed to the difference in the porous structure and packing density of the relevant membranes, as previously reported in other electrospun nanofibrous membrane systems.[9] Moreover, as shown in Table 1, the resultant SiO_2–PEI–PU membranes possess much higher electrolyte uptakes (663.54–795.61%) than Celgard (82.43%) and SiO_2/nylon 6,6 membranes (272–360%),[13] which are consistent with the results of porosities of the relevant membranes, implying that the electrolyte uptake is greatly dependent on the porosity. Meanwhile, the higher electrolyte uptakes of the SiO_2–PEI–PU membranes also originate from the

Table 1 Mean pore sizes, pore size distributions, porosities and electrolyte uptakes of the Celgard membrane and SiO_2–PEI–PU membranes

Samples	Mean pore size (μm)	Pore size distribution (μm)	Porosity (%)	Uptake (%)
Celgard	—	—	49.83	82.43
0 wt% SiO_2	1.81	1.30–2.15	80.66	663.54
2 wt% SiO_2	1.79	1.30–2.15	82.42	681.89
5 wt% SiO_2	1.64	1.15–2.15	83.57	726.63
8 wt% SiO_2	1.59	1.45–2.15	84.97	795.61
11 wt% SiO_2	1.58	1.30–2.10	83.87	714.19

excellent affinity of the carboxyl group (PEI and PU) to the carbonate ester group of the liquid electrolyte.

Ionic conductivity, MacMullin number and tortuosity

It is well known that ionic conductivity is an important factor characterizing the conduction of ionic carriers. Fig. 2 presents the Nyquist plots of the electrochemical impedance for the liquid electrolyte-soaked Celgard membrane and electrospun nanofibrous membranes determined at 25 °C. The intercepts of plots on the real-axis of the liquid electrolyte-soaked membranes represent the bulk resistance. As shown in Table 2, the ionic conductivities of the as-prepared SiO_2–PEI–PU membranes saturated with the electrolyte vary in the range of 1.47–6.25 mS cm^{-1}, which are much higher than that of the Celgard membrane (0.45 mS cm^{-1}). The higher ionic conductivity may be attributed to the higher electrolyte uptake brought about by the higher porosity and the dissociation of PU into the liquid electrolyte.[22] Meanwhile, the Lewis acid–base interactions between the SiO_2 NPs and the electrolyte polar groups also result in an enhancement in ionic conductivity.[25]

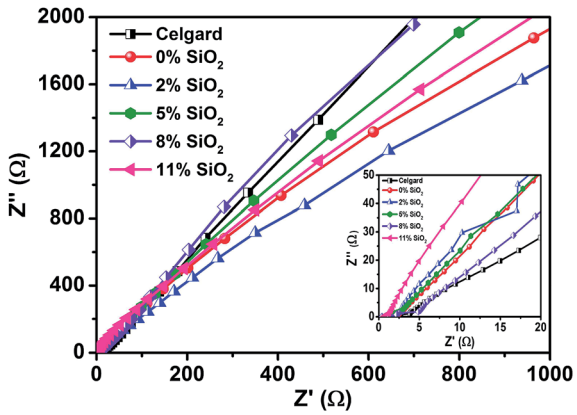

Fig. 2 AC impedance spectra of the liquid electrolyte-soaked Celgard membrane and SiO_2–PEI–PU membranes containing different SiO_2 contents at 25 °C. The inset shows the plots of high-frequency.

In addition, the MacMullin number is known to describe the deterioration of ionic conductivity because of the presence of membranes. The MacMullin numbers of SiO_2–PEI–PU membranes containing 0, 2, 5, 8, and 11 wt% SiO_2 NPs are 5.93, 4.25, 2.62, 1.40, and 2.09, respectively, which are lower than the value of the Celgard membrane (19.38), indicating the lower deterioration of SiO_2–PEI–PU membranes on the battery performance. The MacMullin numbers of SiO_2–PEI–PU membranes are in accordance with their pore size, but for the Celgard membrane, the value is higher than those of the SiO_2–PEI–PU membranes because of its lower porosity although it possesses a smaller pore size.[26]

Besides, tortuosity allows taking into account the impact of the porous structure and porosity on conductivity.[27] The tortuosity values of the resultant SiO_2–PEI–PU membranes are very close, in the range of 1.09–2.19, which are lower than the value of the Celgard membrane (3.11), revealing the higher ionic conductivity of SiO_2–PEI–PU membranes from another point of view. The relatively high ionic conductivities, low MacMullin numbers and tortuosities of the SiO_2–PEI–PU membranes can be attributed to their high porosities (Table 1) with a fully interconnected pore structure (Fig. 1), more electrolyte uptakes (Table 1), and good affinity of PEI and PU to carbonate solvents.

Electrochemical stability window

The electrochemical stability windows of the Celgard and as-prepared SiO_2–PEI–PU membranes evaluated by LSV are shown in Fig. 3. There is no obvious increase in the anodic current below 4.60 V for the Celgard membrane, and the resultant SiO_2–

Table 2 Bulk resistances, ionic conductivities, MacMullin numbers and tortuosities of the Celgard membrane and SiO_2–PEI–PU membranes

Samples	Bulk resistance (Ω)	Ionic conductivity (mS cm^{-1})	MacMullin number	Tortuosity
Celgard	2.2	0.45	19.38	3.11
0 wt% SiO_2	1.7	1.47	5.93	2.19
2 wt% SiO_2	1.22	2.05	4.25	1.65
5 wt% SiO_2	0.74	3.33	2.62	1.67
8 wt% SiO_2	0.4	6.25	1.40	1.09
11 wt% SiO_2	0.6	4.17	2.09	1.75

PEI–PU membranes exhibit higher oxidation potentials in the range of 4.70–4.86 V, revealing that the electrochemical stabilities of SiO_2–PEI–PU membranes are high enough to be used in the high-voltage LIBs. The good electrochemical stabilities of SiO_2–PEI–PU membranes originate from the excellent affinity between the carboxyl group (PEI and PU) and the carbonate ester group of the liquid electrolyte.[28] Furthermore, the improved electrochemical stabilities are also attributed to the stabilizing effect of SiO_2 NPs, which not only absorbs some impurities such as H_2O, HF and O_2, but also reduces side reactions between the electrolyte components and the electrode.[29]

Mechanical strength

The mechanical strength of separators should be strong enough to withstand the tension of the winding operation during battery assembly. As can be seen from Fig. 4a, the tensile strengths of the as-prepared SiO_2–PEI–PU membranes gradually reduce from 8.71 to 6.22 MPa as the SiO_2 content increases; the additions of SiO_2 NPs make the membranes slightly less flexible and thus leading to a decrease in elongation at break. The decrease of the tensile strength could be explained by the fact that the existence of wrinkles, nano protrusions and SiO_2 NPs (Fig. 1) can serve as the points of stress concentration, which become the flaws of SiO_2–PEI–PU membranes and thus deteriorating their tensile strengths. Because of the weak bonding between the loose packing nanofibers, the tensile strengths of SiO_2–PEI–PU membranes are lower than the tensile strength in both the transverse direction (12.88 MPa) and the machine direction (114.28 MPa) of the Celgard membrane (Fig. S1†). Despite that, the tensile strengths of SiO_2–PEI–PU membranes are still higher than those reported in the previous studies.[10,30] Moreover, the SiO_2–PEI–PU membranes containing 8 wt% SiO_2 NPs could be severely twisted several times without breaking along a glass rod with a diameter of 5 mm (Fig. 4b), and not mechanically ruptured after being fully folded at a bending angle of almost 180° (Fig. 4d), reflecting the superior flexibility of the SiO_2–PEI–PU membranes. More notably, the SiO_2–PEI–PU membranes containing 8 wt% SiO_2 NPs can preserve their dimensional stability even after the 400th bending cycle (Fig. 4c). The above results imply that the SiO_2–PEI–PU membranes possess excellent mechanical strength, which could meet the application requirements for high-performance LIBs.

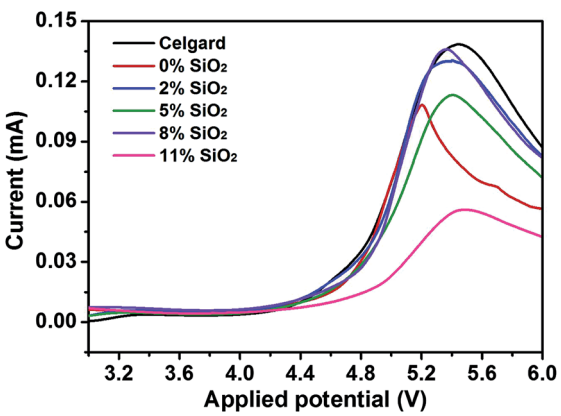

Fig. 3 Electrochemical stability windows of the cells with the Celgard membrane and SiO_2–PEI–PU membranes containing different SiO_2 contents.

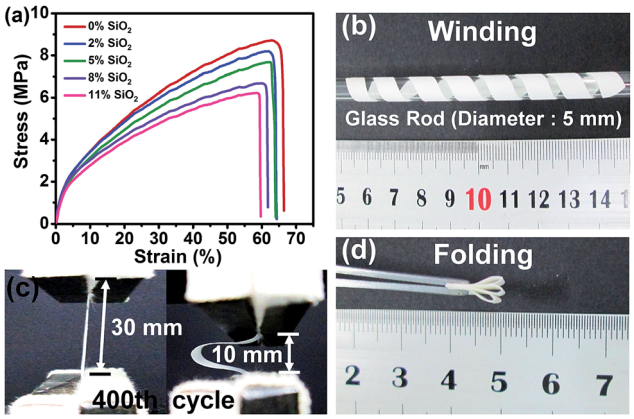

Fig. 4 (a) Stress–strain curves of the as-prepared SiO_2–PEI–PU membranes. Photographs of (b) winding, (c) bending after the 400th cycle, and (d) folding tests of SiO_2–PEI–PU membranes containing 8 wt% SiO_2 NPs.

Dimensional thermal stability and combustion behavior

Dimensional thermal stability is one of the most significant parameters to estimate the safety characteristics of separators. As can be seen in Fig. 5a, it is noted that the Celgard membrane thermally shrinks 15–90% as the temperature increases from 130 to 170 °C, while the dimensional changes of SiO_2–PEI–PU membranes are less than 5% except for the SiO_2–PEI–PU membranes without SiO_2 NPs. As presented in Fig. 5b and c, the Celgard membrane shrinks severely (90%) with the color change from white to transparent, whereas the SiO_2–PEI–PU membranes with 0 wt% SiO_2 NPs shrink by 6% and SiO_2–PEI–PU membranes with 2, 5, 8, and 11 wt% SiO_2 NPs show 2–3% thermal shrinkage at 170 °C for 0.5 h. Based on these results, we can conclude that the SiO_2–PEI–PU membranes exhibit better thermal stability than the Celgard membrane, which could be predominantly ascribed to the incorporation of thermotolerant PEI and SiO_2 NPs. Notably, these results demonstrate that the SiO_2–PEI–PU membranes would prevent thermal shrinkage even at elevated temperature, which is beneficial for improving the safety characteristics of LIBs.

The nonflammable property of separators is another crucial factor for the safety of LIBs, but it has been rarely mentioned because most separators are combustible, except polyimide based membranes,[31] separators prepared using flame retardants or polymers composed of fluorine and bromine functional groups.[32–34] The combustion tests of the Celgard and SiO_2–PEI–PU membranes are shown in Fig. 6, when Celgard is ignited, it is set on fire immediately and is completely engulfed in flames. However, the SiO_2–PEI–PU membranes exhibit perfect flame retarding ability because of the introduction of

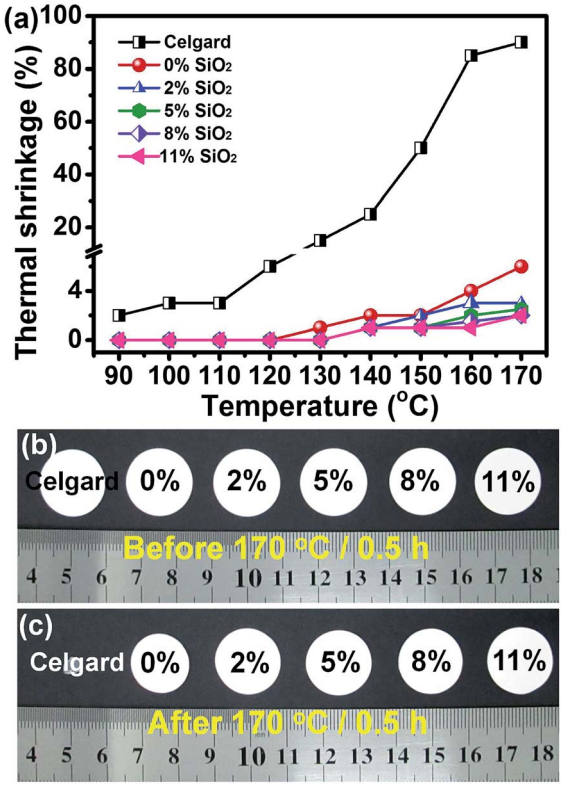

Fig. 5 (a) Comparison of thermal shrinkages of the Celgard membrane and SiO_2–PEI–PU membranes as a function of heat-treatment temperature. Photographs of the Celgard membrane and the as-prepared SiO_2–PEI–PU membranes (b) before and (c) after exposure to 170 °C for 0.5 h.

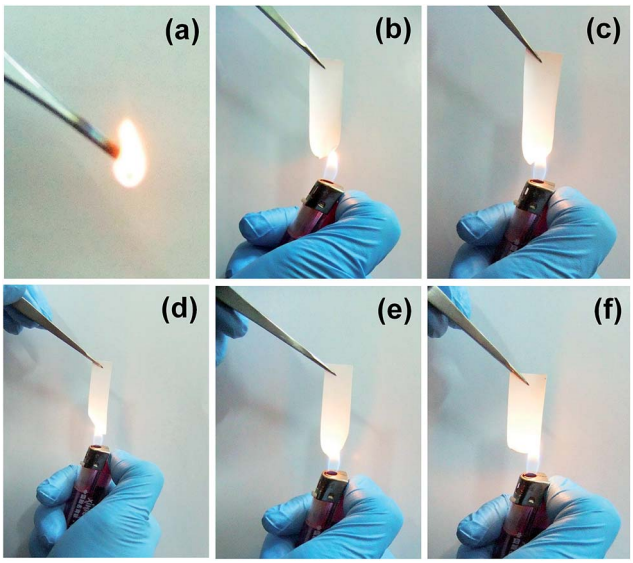

Fig. 6 Combustion tests of (a) Celgard membrane and SiO_2–PEI–PU membranes containing different SiO_2 contents (b) 0 wt%, (c) 2 wt%, (d) 5 wt%, (e) 8 wt% and (f) 11 wt%.

flame retarded PEI and SiO_2 NPs although they shrank. The results are in line with our previous findings indicating that SiO_2–PEI–PU membranes are promising candidates for improving the safety of LIBs.[23]

Cell performance

To further evaluate the applicability of the SiO_2–PEI–PUmembranes as separators for LIBs, the electrochemical behaviors of Li/$LiFePO_4$ coin cells incorporating the high mass loading $LiFePO_4$ electrode of 8 mg cm^{-2} assembled with the relevant membranes and the Celgard membrane were investigated. Fig. 7 illustrates the cyclability of the aforementioned coin cell charge–discharge at 0.2 C for 90 cycles after operating at 0.1 C for 5 cycles, where the coin cells are charged to 4.0 V under a constant current–constant voltage mode, and discharged to 2.5 V in a constant current mode. Fig. 7a–c show the typical charge–discharge profiles of the 1st, 30th, 60th and 90th cycle of the coin cells using the Celgard membrane and SiO_2–PEI–PU membranes containing 0 wt% and 8 wt% SiO_2 NPs, respectively. All the cells exhibit a pair of flat plateaus near 3.38 and 3.5 V, and the cells using the Celgard membrane and SiO_2–PEI–PU membranes containing 0 wt% and 8 wt% SiO_2 NPs deliver initial discharge capacities of 162.25, 162.85 and 166.02 mA h g^{-1}, respectively, the results are consistent with previous reports.[17,35] The difference in discharge capacity is probably due to the difference in the utilization of active materials, after using SiO_2–PEI–PU membranes, the porosity, electrolyte uptake and ionic conductivity increase, and hence more liquid electrolyte can diffuse from the separators to the cathode, which leads to higher utilization of the $LiFePO_4$ active material.[36] However, abnormal charge behaviors are observed in the cells with the Celgard membrane and SiO_2–PEI–PU membranes containing 0 wt% SiO_2 NPs (Fig. 7a and b), which are ascribed to the substantial increase in cell polarization caused by the use of high mass loading of the cathode electrode (8 mg cm^{-2}) and the slower ion transport rate during the charge–discharge reaction.[26] Additionally, the abnormal charge behavior may be attributed to the blocking and penetration effect caused by the dropped electrode particles and the lithium dendrite, which could trigger internal shorting and thus deteriorating battery performance.[37] However, our cell using the Celgard membrane demonstrates higher capacity retention (97%) after 50 cycles than those reported in the previous studies (84% and 87%, respectively).[12,35] Moreover, the cells with the SiO_2–PEI–PU membranes exhibit more stable charge/discharge behavior compared with the cell using the Celgard membrane, especially for the cells with SiO_2–PEI–PU membranes containing 8 wt% and 11 wt% SiO_2 NPs, which deliver a discharge capacity of 158.61 and 158.91 mA h g^{-1} at the 90th cycle (Fig. 7d), respectively. The improvement in cyclability of SiO_2–PEI–PU membranes may be attributed to their tortuously interconnected porous structure (Fig. 1), strong affinity of PEI and PU to the liquid electrolyte (Table 2), as well as the introduction of SiO_2 NPs, as these factors could impart more facile ion transport, higher electrolyte uptake and less adverse reactions during the cycling process.

Fig. 8 compares the discharge capacities of the cells fabricated with different membranes, with the C-rate increasing

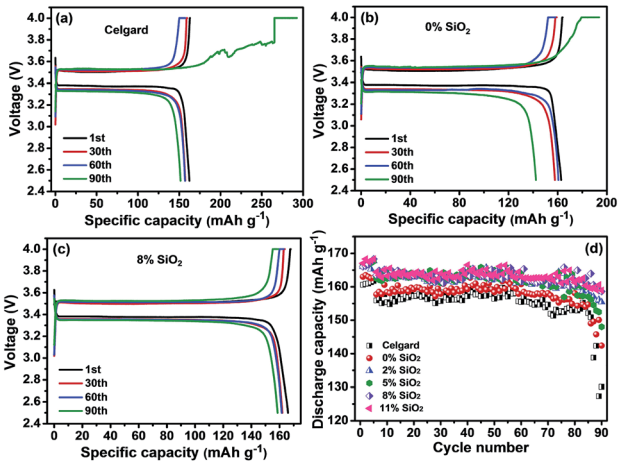

Fig. 7 Charge–discharge profiles of $Li/LiFePO_4$ cells assembled with (a) Celgard membrane and SiO_2–PEI–PU membranes containing (b) 0 wt% and (c) 8 wt% SiO_2 NPs. (d) Cyclability of $Li/LiFePO_4$ cells using the Celgard membrane and SiO_2–PEI–PU membranes containing different SiO_2 contents, charge–discharge at 0.2 C for 90 cycles after operating at 0.1 C for 5 cycles.

from 0.1 C to 1.0 C every 5 cycles. It is notable that the cells with SiO_2–PEI–PU membranes deliver higher discharge capacities at 0.1 C and 0.2 C, and the gaps in discharge capacities increase with increasing current density. Interestingly, when the rate returns to 0.2 C, the reversible discharge capacities of the above-mentioned cells were both close to the original rate capacity of 0.2 C, indicating that the structural stabilities of the cathode materials are retained.[17] The capacity retention ratios (calculated based on the initial discharge capacity) of the cell assembled with the Celgard membrane and SiO_2–PEI–PU membranes containing 0, 2, 5, 8, and 11 wt% SiO_2 NPs at the 20th cycle (1.0 C) are 68.23%, 79.38%, 81.58%, 83.03%, 88.53%, and 86.45%, respectively. The cells using SiO_2–PEI–PU membranes containing 8 wt% SiO_2 NPs exhibit better rate capability not only than the other cells using SiO_2–PEI–PU membranes but also than the cells using SiO_2/PEI–PU membranes in our previous study.[23] Notably, it seems a paradoxical phenomenon that the capacity retention ratios are more than 100% at 0.1 C on occasion, which is attributed to the formation of a solid electrolyte interface film during initial cycles. The improved discharge C-rate capability of the cell with SiO_2–PEI–PU membranes, especially at a higher rate, can be explained by their higher ionic conductivities caused by the synergetic effect of PEI, PU and SiO_2 NPs, which reduce the concentration polarization of the electrolyte and thus deliver higher discharge capacity.

Considering the volatilization of the liquid electrolyte and the thermal decomposition of $LiPF_6$, high temperature cell performances of the $Li/LiFePO_4$ cells using SiO_2–PEI–PU and Celgard membranes have been tested at 0.2 C till 25 cycles after operating at 0.1 C for 5 cycles at 60 °C. As demonstrated in Fig. 9a, the cell using the SiO_2–PEI–PU membranes containing 8 wt% SiO_2 NPs shows more stable cyclability, delivering a capacity retention of 99.6% after 25 cycles. Moreover, the cell

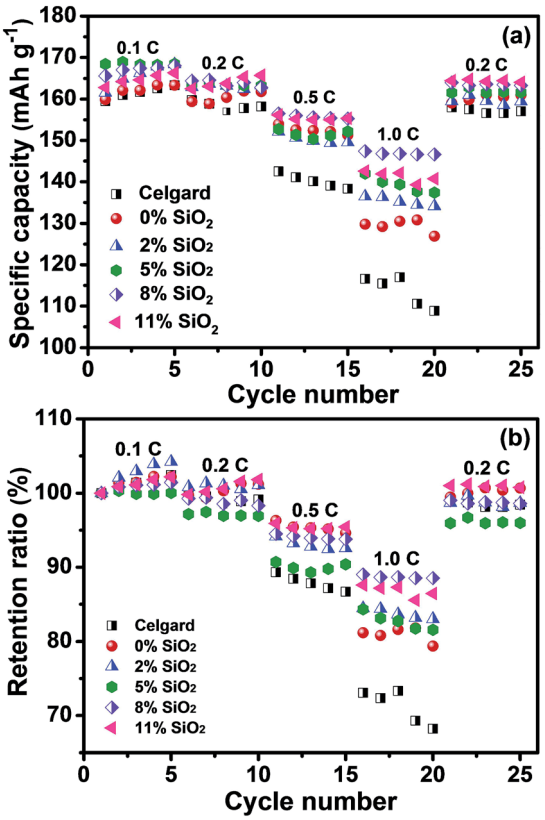

Fig. 8 (a) Comparison of discharge rate capabilities of $Li/LiFePO_4$ cells using the Celgard membrane and SiO_2–PEI–PU membranes at different C-rates. (b) Capacity retention of $Li/LiFePO_4$ cells using the Celgard membrane and SiO_2–PEI–PU membranes at different C-rates.

based on the SiO_2–PEI–PU membranes containing 8 wt% SiO_2 NPs exhibits better rate capability as shown in Fig. 9b. Even at a high discharge current density (1.0 C rate), the cell exhibits a discharge capacity up to 128.3 mA h g^{-1}, which maintains 82.3% of the initial capacity at 0.1 C rate. The excellent discharge performance of the SiO_2–PEI–PU composite membranes may be ascribed to the good ability to retain the electrolyte solution at a high temperature. Benefiting from the good electrolyte retaining ability and the high heat resistance at elevated temperature, the SiO_2–PEI–PU membranes would enhance the safety characteristics of high power LIBs.

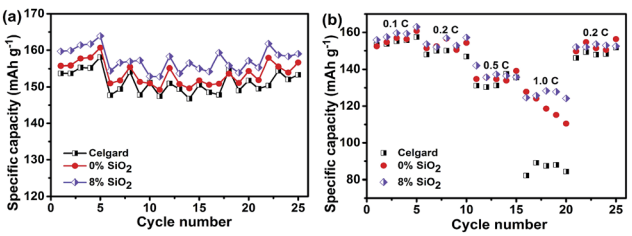

Fig. 9 (a) Cyclability and (b) rate capability of the $Li/LiFePO_4$ cells using the Celgard membrane and SiO_2–PEI–PU membranes at an elevated temperature of 60 °C.

Conclusions

In conclusion, SiO_2–PEI–PU membranes have been successfully constructed *via* an electrospinning technique, which has been shown to possess superior ionic conductivity and excellent safety for use in high power LIBs. Owing to the introduction of SiO_2 NPs, high porosity and electrolyte uptake, the SiO_2–PEI–PU membranes were endowed with a superior ionic conductivity of 6.25 mS cm^{-1}, a high anodic stability up to 4.86 V, uniform pore size distribution and improved thermostability displaying 2% dimensional change after exposure to 170 °C for 0.5 h. Notably, the Li/$LiFePO_4$ (high mass loading $LiFePO_4$ electrode of 8 mg cm^{-2}) coin cells based on the as-prepared SiO_2–PEI–PU membranes exhibit higher cyclability and better rate capability compared with the Celgard membrane based cell not only at room temperature but also at elevated temperature, indicating that the SiO_2–PEI–PU membranes are potential separator candidates for high power LIBs. The results in this work encourage us to continue the study on high-performance LIBs with the aim of achieving high cyclability and rate capability by applying electrospun nanofibrous membranes as separators.

Acknowledgements

This work is supported by the Shanghai Committee of Science and Technology (no. 12JC1400101), the National Natural Science Foundation of China (no. 51322304), the Fundamental Research Funds for the Central Universities, and the "DHU Distinguished Young Professor Program".

Notes and references

1 P. Arora and Z. Zhang, *Chem. Rev.*, 2004, **104**, 4419.
2 H. Lee, M. Yanilmaz, O. Toprakci, K. Fu and X. Zhang, *Energy Environ. Sci.*, 2014, **7**, 3857.
3 C. M. Costa, M. M. Silva and S. Lanceros-Méndez, *RSC Adv.*, 2013, **3**, 11404.
4 C. J. Orendorff, T. N. Lambert, C. A. Chavez, M. Bencomo and K. R. Fenton, *Adv. Energy Mater.*, 2013, **3**, 314.
5 W. Chen, Y. Liu, Y. Ma and W. Yang, *J. Power Sources*, 2015, **273**, 1127.
6 Q. Wang, W. L. Song, L. Wang, Y. Song, Q. Shi and L. Z. Fan, *Electrochim. Acta*, 2014, **132**, 538.
7 W. Li, Y. Xing, Y. Wu, J. Wang, L. Chen, G. Yang and B. Tang, *Electrochim. Acta*, 2015, **151**, 289.
8 R. Zhou, W. Liu, J. Kong, D. Zhou, G. Ding, Y. W. Leong, P. K. Pallathadka and X. Lu, *Polymer*, 2014, **55**, 1520.
9 Y. Zhai, N. Wang, X. Mao, Y. Si, J. Yu, S. S. Al-Deyab, M. El-Newehy and B. Ding, *J. Mater. Chem. A*, 2014, **2**, 14511.
10 X. Huang, *J. Membr. Sci.*, 2014, **466**, 331.
11 H. Bi, G. Sui and X. Yang, *J. Power Sources*, 2014, **267**, 309.
12 M. Rao, X. Geng, Y. Liao, S. Hu and W. Li, *J. Membr. Sci.*, 2012, **399–400**, 37.
13 M. Yanilmaz, M. Dirican and X. Zhang, *Electrochim. Acta*, 2014, **133**, 501.
14 X. Wang, B. Ding and B. Li, *Mater. Today*, 2013, **16**, 229.
15 X. Wang, B. Ding, G. Sun, M. Wang and J. Yu, *Prog. Mater. Sci.*, 2013, **58**, 1173.
16 J. Lin, X. Wang, B. Ding, J. Yu, G. Sun and M. Wang, *Crit. Rev. Solid State Mater. Sci.*, 2012, **37**, 94.
17 M. Raja, N. Angulakshmi, S. Thomas, T. P. Kumar and A. M. Stephan, *J. Membr. Sci.*, 2014, **471**, 103.
18 J. Fang, A. Kelarakis, Y. W. Lin, C. Y. Kang, M. H. Yang, C. L. Cheng, Y. Wang, E. P. Giannelis and L. D. Tsai, *Phys. Chem. Chem. Phys.*, 2011, **13**, 14457.
19 K. J. Kim, H. K. Kwon, M. S. Park, T. Yim, J. S. Yu and Y. J. Kim, *Phys. Chem. Chem. Phys.*, 2014, **16**, 9337.
20 S. O. Han, W. K. Son, D. Cho, J. H. Youk and W. H. Park, *Polym. Degrad. Stab.*, 2004, **86**, 257.
21 H. Fashandi and M. Karimi, *Ind. Eng. Chem. Res.*, 2013, **53**, 235.
22 L. Zhou, Q. Cao, B. Jing, X. Wang, X. Tang and N. Wu, *J. Power Sources*, 2014, **263**, 118.
23 Y. Zhai, K. Xiao, J. Yu and B. Ding, *Electrochim. Acta*, 2015, **154**, 219.
24 K. H. Choi, S. J. Cho, S. H. Kim, Y. H. Kwon, J. Y. Kim and S. Y. Lee, *Adv. Funct. Mater.*, 2014, **24**, 44.
25 Y. J. Kim, C. H. Ahn, M. B. Lee and M. S. Choi, *Mater. Chem. Phys.*, 2011, **127**, 137.
26 J. H. Kim, J. H. Kim, K. H. Choi, H. K. Yu, J. H. Kim, J. S. Lee and S. Y. Lee, *Nano Lett.*, 2014, **14**, 4438.
27 I. V. Thorat, D. E. Stephenson, N. A. Zacharias, K. Zaghib, J. N. Harb and D. R. Wheeler, *J. Power Sources*, 2009, **188**, 592.
28 H. R. Jung and W. J. Lee, *Electrochim. Acta*, 2011, **58**, 674.
29 Y. Liao, C. Sun, S. Hu and W. Li, *Electrochim. Acta*, 2013, **89**, 461.
30 N. Angulakshmi and A. Manuel Stephan, *Electrochim. Acta*, 2014, **127**, 167.
31 B. Zhang, Q. Wang, J. Zhang, G. Ding, G. Xu, Z. Liu and G. Cui, *Nano Energy*, 2014, **10**, 277.
32 J. Zhang, L. Yue, Q. Kong, Z. Liu, X. Zhou, C. Zhang, Q. Xu, B. Zhang, G. Ding, B. Qin, Y. Duan, Q. Wang, J. Yao, G. Cui and L. Chen, *Sci. Rep.*, 2014, **4**, 3935.
33 Y. Zhu, S. Xiao, Y. Shi, Y. Yang, Y. Hou and Y. Wu, *Adv. Energy Mater.*, 2014, **4**, 1300647.
34 J. Woo, S. Nam, S. Seo, S. Yun, W. Kim, T. Xu and S. Moon, *Electrochem. Commun.*, 2013, **35**, 68.
35 J. Hao, G. Lei, Z. Li, L. Wu, Q. Xiao and L. Wang, *J. Membr. Sci.*, 2013, **428**, 11.
36 R. Prasanth, V. Aravindan and M. Srinivasan, *J. Power Sources*, 2012, **202**, 299.
37 J. Zhang, L. Yue, Q. Kong, Z. Liu, X. Zhou, C. Zhang, S. Pang, X. Wang, J. Yao and G. Cui, *J. Electrochem. Soc.*, 2013, **160**, A769.

